Design and Implementation of a Controller for Navigating an Autonomous Ground Vehicle

Shubhashisa Sahoo, Shankar C. Subramanian, *Member, IEEE,* and Suresh Srivastava

***Abstract*-- This paper describes the design and implementation of a heading controller for an autonomous ground vehicle (AGV) taking into account the vehicle dynamics. The challenge in designing this control system is to choose a dynamic model that is sufficiently valid for a typical road vehicle. The well-known "bicycle model" approximation has been used that considers the vehicle slip angle and ground-wheel interaction for the wheeled ground vehicle. In this paper, both proportional and proportional-integral (PI) controllers have been designed, simulated and implemented to achieve the desired heading angle. Results from both simulation and experimental implementation are compared. It has been found that the vehicle controller can be tuned effectively to achieve the desired heading change of twenty degrees within six seconds when the vehicle is moving at a speed of 1 m/sec.**

***Index Terms*—Land vehicles, navigation, path tracking, proportional control, PI control.**

I. Nomenclature

m	–	Mass of the vehicle
I_z	–	Yaw moment of inertia of the vehicle
δ	–	Steering angle of the front wheel
r	–	Yaw rate of the vehicle
θ	–	Vehicle yaw angle measured w.r.t global X-axis
$\mathbf{v}$	–	Velocity of the vehicle
F_{yf}	–	Lateral tire force on the front wheel
F_{yr}	–	Lateral tire force on the rear wheel
l	–	Wheelbase
l_f	–	Distance of the front tire from vehicle CG
l_r	–	Distance of the rear tire from vehicle CG
w	–	Track width
C_f	–	Cornering stiffness for the front wheel
C_r	–	Cornering stiffness for the rear wheel

II. Introduction

A significant task in designing controllers for an autonomous ground vehicle (AGV) involves the design and development of path trackers. A path tracker is a system that applies appropriate steering motions to guide the vehicle along the path as described by the vehicle path planner. For a typical patrol mission scenario, the path can be obtained in several ways. Several solutions to this problem have been proposed in the literature [1], [2]. Indeed, feasible reactive trajectories in real time can be generated in response to newly acquired environmental information [3].

In principle, a path should be defined as a continuous function. In practice, however, it is discretized and described either as a series of straight line segments between interim goal waypoints or as a series of closely spaced nodes typically spaced tens to hundreds of meters apart, as shown in Fig. 1.

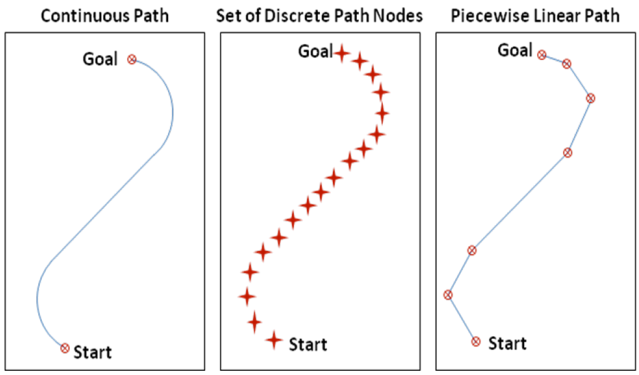

Fig. 1. Various ways of defining the path.

If the path is specified as a series of straight line segments, the algorithm will attempt to follow these straight lines. If it is specified as a series of closely spaced nodes, the algorithm will only attempt to attain the next node. Waypoints are sent to the AGV as a set of positions, in latitude and longitude coordinates, accompanied by a radial tolerance for each. For a waypoint to have been reached, the vehicle must pass it at a distance less than or equal to the radial tolerance for that waypoint. The straight line segment between the previous waypoint and the next waypoint will be the path tracked by the algorithm.

Even in the absence of obstacles, there is no general algorithm to plan motions for any nonholonomic system so that the system is guaranteed to exactly reach a given goal [4]. The only existing results are for approximate methods, which only guarantee that the system reaches a neighborhood of the goal. Obstacle avoidance adds a second level of difficulty. Particularly, a car-like robot has only two controls (linear and angular velocities) while it moves in a 4-dimensional configuration space (x, y, θ and ρ) where (x, y) are the coordinates of a reference point of the vehicle, θ is the orientation of the vehicle and ρ is the instantaneous curvature of the path. The admissible paths are generated by a sequence of these inputs, each of them being applied over a fixed

Shubhashisa Sahoo is with the Centre for Artificial Intelligence and Robotics, Bangalore, 560093, INDIA (e-mail: shubhashisa@cair.drdo.in).

Shankar C. Subramanian (corresponding author) is with the Department of Engineering Design, Indian Institute of Technology Madras, Chennai, 600036, INDIA (e-mail: shankarram@iitm.ac.in).

Suresh Srivastava is with the Gas Turbine Research Establishment, Bangalore, 560093, INDIA (e-mail: sureshsrivastava@gtre.drdo.in).

978-1-4673-1049-9/12/$31.00 ©2012 IEEE

interval of time, δt. As a consequence, the control algorithm developed for holonomic systems does not apply directly to nonholonomic ones.

Using the concept of the look-ahead distance, there are many different types of path tracking algorithms available today. Three popular algorithms are follow-the-carrot [5], pure pursuit [6] and vector pursuit [7]. The first two methods have been around for quite a while now, while vector pursuit or screw tracking, as it is also called, is relatively new. The main difference between these methods is that vector pursuit uses information about orientation at the look-ahead point, while the others do not [8].

However, in all these geometric techniques, the performance was found to be overly dependent on the look-ahead point, which is on the planned path at a distance D from the vehicle, to determine the desired motion of the vehicle. Unfortunately, there is a tradeoff in determining the distance D and the vehicle speed. As the vehicle speed increases, the look-ahead distance typically needs to be increased, too [9]. Furthermore, these models do not either consider the vehicle slip angle or the restriction on the vehicle steering which cannot be ignored for an AGV. Consequently, the planned path becomes unusable for the mission achievement. So, to bridge a gap between planning and navigation, a realistic control strategy has been proposed in this paper based on a dynamic bicycle vehicle model [10]. The details of the model and the controller are presented in sections III and IV respectively. The controller performance has been compared with experiments in section IV and concluding remarks are provided in section V.

III. DYNAMIC MODELING OF THE SYSTEM

A simple approximation of the lateral dynamics of land vehicles is the "bicycle model" [10]. This approximation combines the effects of the two front wheels and treats them as a single wheel. The bicycle model also combines the two rear wheels and treats them as a single wheel.

A. Linearized Dynamic Bicycle Model

A linearized model, often sufficient to provide satisfactory performance in the operating range of interest, is widely used in control system design. In most land vehicle control applications, a linear and time invariant (LTI) model is used. A bicycle model of the vehicle with two degrees of freedom, as shown in Fig. 2, is considered in this study.

The two degrees of freedom are represented by the vehicle lateral position, y, and the vehicle yaw angle, θ. The vehicle lateral position is measured along the lateral axis of the vehicle and the vehicle yaw angle is measured with respect to the global X-axis. The lateral force at the tire-road interface depends on the slip angle. Figure 2 illustrates the bicycle model for a vehicle with no roll motion. It is assumed that only the front wheel is steerable. The lateral motion of the vehicle is described by

$$m\dot{v}_y = F_{xf}\sin\delta + F_{yf}\cos\delta + F_{yr} \tag{1}$$

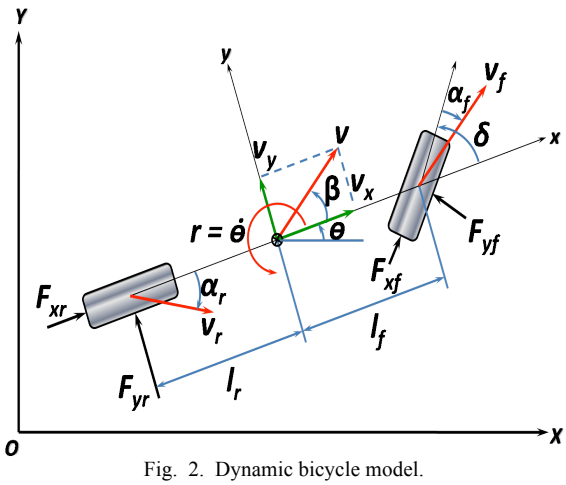

Fig. 2. Dynamic bicycle model.

The equation governing the yaw motion is

$$I_z\dot{r} = l_f F_{xf}\sin\delta + l_f F_{yf}\cos\delta - l_r F_{yr} \tag{2}$$

Considering δ to be small, (1) and (2) can be written as

$$ma_y = F_{yf} + F_{yr} \tag{3}$$

$$I_z\dot{r} = l_f F_{yf} - l_r F_{yr} \tag{4}$$

The velocity vector **v** can be written as

$$\mathbf{v} = v_x\mathbf{i} + v_y\mathbf{j} \tag{5}$$

where **i** and **j** are the unit vectors in x and y directions respectively. Here, v_x and v_y are the velocity components in the x and y directions respectively. The x–y coordinate system is fixed to the vehicle. The acceleration could be written as

$$\mathbf{a} = (\dot{v}_x - v_y r)\mathbf{i} + (\dot{v}_y + v_x r)\mathbf{j} \tag{6}$$

Substituting y-component of the acceleration from (6) into (3), the lateral motion of the vehicle is described by

$$m(\dot{v}_y + v_x r) = F_{yf} + F_{yr} \tag{7}$$

Experimental results show that the lateral tire force of a tire is proportional to the slip-angle for small slip-angles [11]. The slip angle of a tire is defined as the angle between the orientation of the tire and the orientation of the velocity vector of the wheel as shown in Fig. 3.

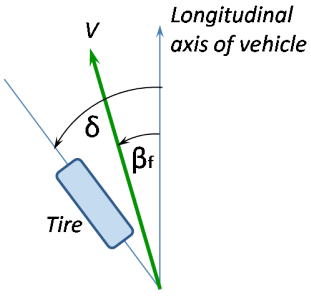

Fig. 3. Tire slip-angle.

The slip angles of the front and rear wheels are

$$\alpha_f = \delta - \beta_f \tag{8}$$

$$\alpha_r = -\beta_r \tag{9}$$

where β_f and β_r are the angles that the velocity vectors of the front and rear wheels make with the longitudinal axis of the vehicle respectively. When a side-slip angle is negative, F_{yf} and F_{yr} act in the positive y-direction. For small slip angles, the lateral forces acting on the front and rear wheels can be written as

$$F_{yf} = C_f \alpha_f \tag{10}$$

$$F_{yr} = C_r \alpha_r \tag{11}$$

The side-slip angles are given by

$$\tan \beta_f = \frac{v_y + l_f r}{v_x} \quad \text{or} \quad \beta_f \approx \frac{v_y + l_f r}{v_x} \tag{12}$$

Substituting β_f from (12) in (8) results in

$$\alpha_f = \delta - \left(\frac{v_y + l_f r}{v_x} \right) \tag{13}$$

Similarly, the slip angle for rear wheel can be written as

$$\alpha_r = -\left(\frac{v_y - l_r r}{v_x} \right) \tag{14}$$

Using (10), (11), (13) and (14), the governing equations (4) and (7) become

$$m\dot{v}_y + \left(\frac{C_f + C_r}{v_x} \right) v_y + \left(m v_x + \frac{C_f l_f - C_r l_r}{v_x} \right) r = C_f \delta \tag{15}$$

$$I_z \dot{r} + \left(\frac{C_f l_f - C_r l_r}{v_x} \right) v_y + \left(\frac{C_f l_f^2 + C_r l_r^2}{v_x} \right) r = C_f l_f \delta \tag{16}$$

The transfer function, $G_\delta^r(s)$, which is the response of yaw rate to the steering angle, is obtained as

$$G_\delta^r(s) = \frac{a_{r1} s + a_{r2}}{s^2 + 2\xi\omega_n s + \omega_n^2} \tag{17}$$

where $a_{r1} = \frac{C_f l_f}{I_z}$, $a_{r2} = \frac{C_f C_r l}{m I_z v_x}$,

$$2\xi\omega_n = \frac{m\left(C_f l_f^2 + C_r l_r^2\right) + I_z\left(C_f + C_r\right)}{m I_z v_x},$$

$$\omega_n^2 = \frac{C_f C_r l^2}{m I_z v_x^2} - \frac{\left(C_f l_f - C_r l_r\right)}{I_z}.$$

The transfer function, $G_\delta^\theta(s)$, which is the response of heading angle to the steering angle, is obtained as

$$G_\delta^\theta(s) = \frac{a_{r1} s + a_{r2}}{s\left(s^2 + 2\xi\omega_n s + \omega_n^2\right)} \tag{18}$$

B. Controller for Desired Heading

Let us consider a closed-loop negative feedback system for tracking the yaw angle as shown in Fig. 4. Its close loop transfer function is given by

$$\frac{\theta(s)}{\theta_{des}(s)} = \frac{G_\delta^\theta(s) H_\delta^\theta(s)}{1 + G_\delta^\theta(s) H_\delta^\theta(s)} \tag{19}$$

where $H_\delta^\theta(s)$ is the transfer function for the controller.

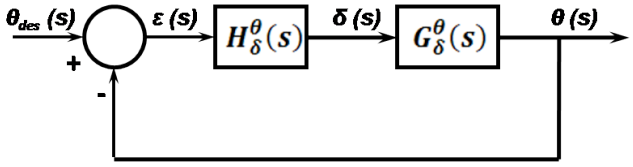

Fig. 4. Negative feedback system for desired heading.

C. Test Platform

In order to implement and verify the proposed control strategies, a commercial electric vehicle, CARRIEALL car was modified to fulfill the experimental requirements. The electric cart is equipped with a 3 kW DC motor and a self-adjusting rack and pinion steering. The front body of the vehicle is modified to provide the space for mounting of sensors and cameras. The primary means of localization will be satellite based, such as by a Global Positioning System (GPS). To cater for likely eventualities such as GPS inaccuracy, outage or denial, the system will also have an accurate Inertial Navigation System (INS) onboard, which will augment and be augmented by the GPS. The INS comprises an odometer, compass and Inertial Measurement Unit (IMU). The test platform after modification and mounting of equipment is shown in Fig. 5.

Fig. 5. Test platform.

The drive system of the vehicle consists of two motors. A 3kW DC motor is used to accelerate and decelerate the vehicle in the longitudinal direction. Another DC motor (Maxon RE-40) with a 156:1 reduction gear ratio is installed at the steering rod for controlling the heading direction. This motor is connected to the steering shaft with the help of spur gears. The rotation of the steering shaft can be measured by the encoder attached to the steering motor.

D. Model Parameter Identification

The dynamic bicycle model has parameters that are not directly measureable. However, a workable estimate can be obtained using commonly available tools. The measurement of the vehicle's split mass, utilizing four scales under each wheel, is necessary to estimate the vehicle's total mass, C.G. location and moment of inertia. The total mass of the vehicle is simply the sum of the measurements of mass under each wheel of the vehicle given by

$$m = m_{fl} + m_{fr} + m_{rl} + m_{rr} \tag{20}$$

where m_{fl}, m_{fr}, m_{rl}, and m_{rr} are the mass of the vehicle at front-left, front-right, rear-left and rear-right respectively. Given the modelling of the front and rear wheels as a single wheel at the center of each axle, an assumption is also made that the vehicle's mass is laterally evenly distributed. The front wheel mass, m_f and the rear wheel mass, m_r are given by

$$m_f = m_{fl} + m_{fr} \quad \text{and} \quad m_r = m_{rl} + m_{rr}$$

From this and a measurement of the wheel base l, the location of the vehicle's C.G., described by distances l_f and l_r from the front and rear axles along the center line can be estimated as

$$l_f = l\left(1 - \frac{m_f}{m}\right) \quad \text{and} \quad l_r = l\left(1 - \frac{m_r}{m}\right)$$

The vehicle's moment of inertia is approximated by treating the vehicle as two point masses joined by a mass-less rod. The moment of inertia for the vehicle is then given as

$$I_z = m_f l_f^2 + m_r l_r^2 \tag{21}$$

Finally, the cornering stiffness parameters C_f and C_r must be identified. These parameters can be obtained from data sheets produced for the specific tire. As cornering stiffness parameters C_f and C_r are not readily available for this vehicle, it is normalized by the vertical load. At 1^0 of slip angle, the average bias tire will produce a lateral force of 10 % of the vertical load. On average, radial tires have a higher cornering stiffness than bias-ply-tires [12]. For radial tires, it is considered that cornering stiffness per degree of slip angle is approximately 16 - 17 % of the load on the tire [12]. Thus,

$$\begin{aligned} C_f &= m_f * g * 0.165(N/\deg) \\ C_r &= m_r * g * 0.165(N/\deg) \end{aligned} \tag{22}$$

The specification data for the test vehicle considered here are listed in Table I.

TABLE I
PARAMETERS OF THE TEST VEHICLE

Parameter	Value
l	1.93 m
w	0.90 m
l_f	1.31 m
l_r	0.62 m
m_{fl}	158 kg
m_{fr}	137 kg
m_{rl}	360 kg
m_{rr}	269 kg
I_z	932.4 kg.m2
C_f	27359 N/rad
C_r	58335 N/rad

IV. IMPLEMENTATION AND EXPERIMENTAL RESULTS

The control system has been tested for tracking a step input of 20^0 yaw angle with a maximum overshoot of 10 % and a settling time less than 6 sec. The longitudinal velocity of the vehicle has been kept constant at 1 m/sec. The control gains that would place the closed loop poles in the desired locations (corresponding to the above performance specifications) have been analytically determined and subsequently used in the experimental implementation. Substituting the values of the vehicle parameters from Table 1 in (18), the transfer function, $G_\delta^\theta(s)$ is obtained as

$$G_\delta^\theta(s) = \frac{38.55(s+92.74)}{s(s+74.40)(s+92.74)} \tag{23}$$

The common pole-zero pair at –92.74 can be cancelled here, and thus, (23) can be written as

$$G_\delta^\theta(s) = \frac{38.55}{s(s+74.40)} \tag{24}$$

A. Proportional Controller

Considering a proportional controller,

$$H_\theta^\delta(s) = K_p \tag{25}$$

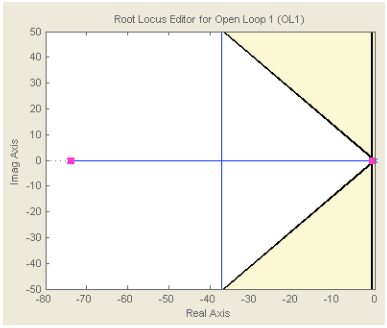

Fig. 6. Root Locus of the closed loop poles.

The maximum overshoot requirement of 10 % of steady state response results in the damping ratio, ζ, being less than 0.6. The desired region of the closed loop poles is shown in Fig. 6. The characteristic equation for this negative closed loop feedback system is

$$s^2 + 74.4s + 38.55K_p = 0 \tag{26}$$

The value of K_p calculated at the pole location of -0.67 (which satisfies the performance requirements) was found to be 1.27. For this value, the yaw angle tracking response has been simulated using MATLAB-Simulink and the corresponding diagram is shown in Fig. 7.

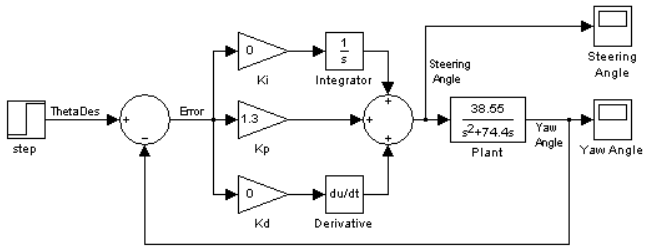

Fig. 7. MATLAB-Simulink diagram to simulate the yaw angle response

The steering angle input from the simulation is shown in Fig. 8. For a desired step input yaw angle of 20^0, considering that the vehicle is moving at a constant velocity of 1 m/sec, the maximum steering angle input required is 25^0, which is within the vehicle steering limit of 35^0.

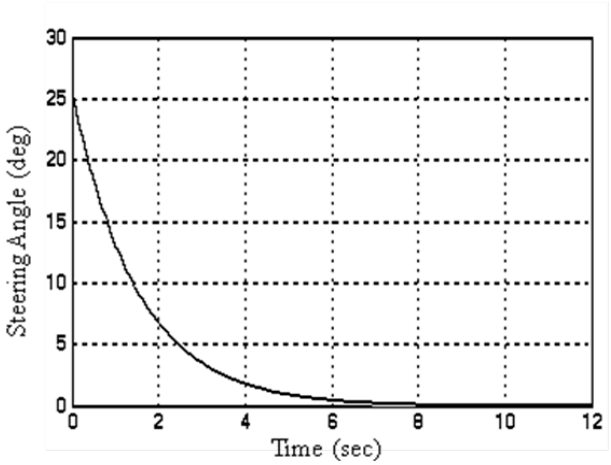

Fig. 8. Steering angle response $K_p = 1.27$

Several tests have been made to check the theoretical results explained in the preceding sections. These tests have been carried out on the test platform (shown in Fig. 5.) In each test performed, the vehicle was commanded to achieve a constant forward velocity of 1 m/sec and then follow a heading angle of 20^0. To compare the simulated with the experimental result, the closed-loop yaw angle response with $K_p = 1.2$ has been plotted in Fig. 9. To start with, the test was first carried out for $K_p = 1.2$, then increased up to 1.5 and the results are plotted in Fig. 10.

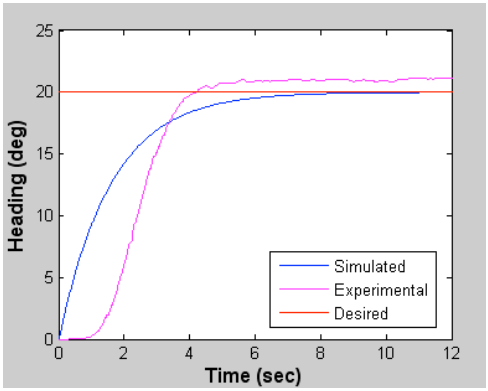

Fig. 9. Comparison of simulated and experimental result with proportional controller with $Kp = 1.2$

As shown in Fig. 9, for $K_p = 1.2$, the desired heading can be achieved in less than 6 sec with some steady state error. For a better understanding of the system behavior and to reduce the settling time, the yaw response has been plotted for different values of K_p and the results are shown in Fig. 10.

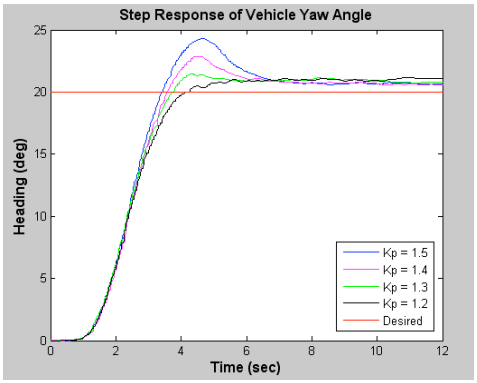

Fig. 10. Step response of vehicle yaw angle with different values of K_p

B. *Proportional and Integral (PI) Controller*

Integral control bases its corrective action on the cumulative error integrated over time and is used to eliminate the steady state errors. For a Proportional Integral (PI) controller

$$H_{\theta}^{\delta}(s) = K_p + \frac{K_I}{s} = \frac{K_P(s+Z_0)}{s} \qquad (27)$$

where $Z_0 = K_I / K_p$. As (27) shows, the controller adds a pole at the origin as well as a zero at $-Z_0$, which is influenced by the choice of K_I and K_p. In order to satisfy the performance requirements, it was determined that $-Z_0$ should be close to the origin. Therefore, the integral gain should be small compared to the proportional gain.

For the PI controller, simulation has been carried out in MATLAB using control and estimation tools manager. Considering K_I to be *0.01*, it has been found that for $K_p = 1.7$, the required steering angle is very close to 35^0 as shown in Fig. 11, which is within the maximum steering limit. By increasing the value of K_p beyond 1.7, the overshoot can be reduced to achieve the desired settling time. However, the required steering angle of the front wheel will exceed the maximum steering limit.

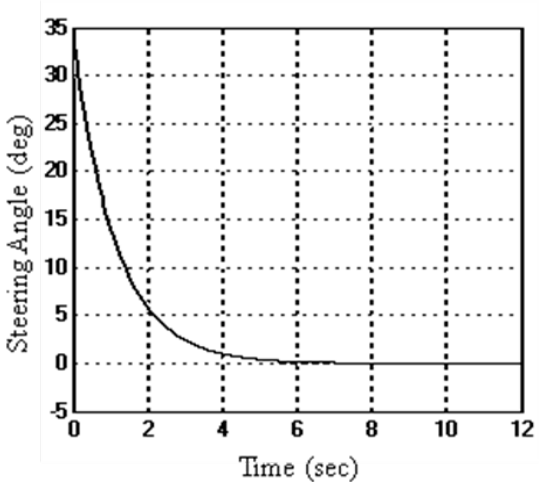

Fig. 11. Steering angle response for $K_p = 1.7$ and $K_I = 0.01$

To compare the simulation result with the experimental results, several tests have been carried out for different values of K_p keeping $K_I = 0.01$. Both the simulated and experimental closed-loop yaw angle responses for $K_p = 1.7$ have been plotted in Fig. 12. In each of the tests performed, the vehicle

was commanded to achieve a constant forward velocity of 1 m/sec and then follow a heading angle of 20^0. The yaw angle responses with varying K_p have been plotted in Fig. 13.

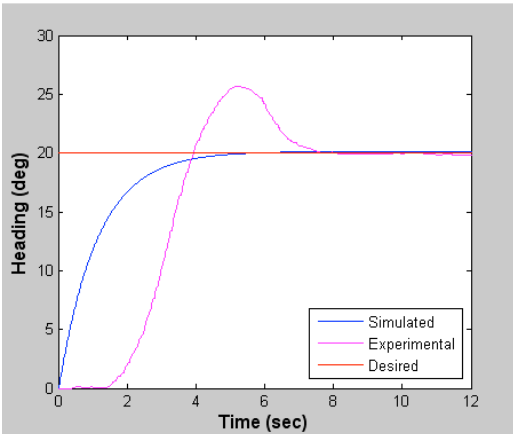

Fig. 12. Comparison of Simulated and experimental result with PI controller with Kp = 1.7 and K_I = 0.01

As shown in Fig. 12, when K_p = 1.7 and K_p = 0.01, the desired heading can be achieved in less than 8 sec with no steady state error. However, the difference in the simulated and experimental yaw response can be minimized by considering the time delay and experimentally estimating the cornering stiffness of the tires. Theoretically, the settling time and overshoot can be reduced by increasing K_p, but it is difficult to implement as the required steering angle is restricted by the physical steering limit. As shown in Fig. 13, the system starts oscillating for K_p = 2.0. For better understanding of the system behavior, the yaw response has been plotted by varying the values of K_p and plotted in Fig. 13.

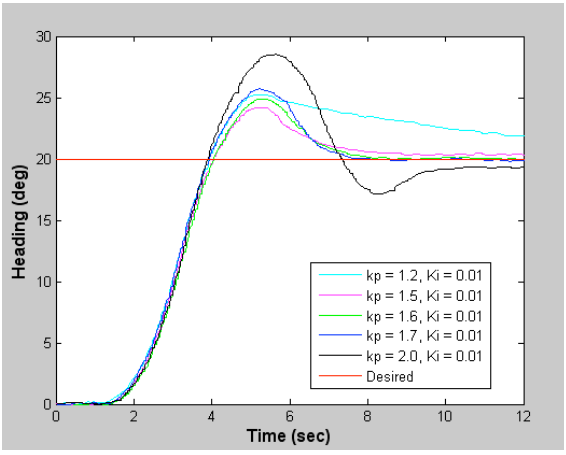

Fig. 13. Step response of vehicle yaw angle with PI controller

V. CONCLUSIONS

This paper proposed the use of the dynamic bicycle model for path tracking of an autonomous ground vehicle equipped with IMU and GPS. Any robotic mission specified as a sequence of waypoints could be tracked using these control strategies. The proposed proportional and PI controllers have followed desired heading angle in a reliable and smooth way in an outdoor environment. When the vehicle is moving at a constant velocity of 1m/sec, a heading angle change of 20^0 can be achieved within 5 seconds with 5% steady state error using the proportional controller. However, the steady state error can be eliminated using the PI controller, but it increases the settling time and maximum overshoot. In this way, the vehicle can be navigated closely to the path to be followed.

Perhaps, the most exciting issues come from the experimental data and practical applications. The gap between the model and the real world is critical. Several experiments have been carried out with the test vehicle to compare with the simulated results. Moreover, the influence of design parameters has also been studied experimentally. The difference in the simulated and experimental results may due to the following reasons:

- Approximation in estimating the cornering stiffness of front and rear tires.
- Motor rate limits and latency must be modeled in order to produce an accurate simulation.

For future work, the system model has to be modified to include the steering wheel's response to rotation of steering motor. The dynamics of the actuator must be incorporated and schemes to estimate unknown parameters such as the cornering stiffness must be developed.

VI. REFERENCES

[1] J. Barraquand and J. C. Latombe, "On nonholonomic mobile robots and optimal maneuvering," *Proc. of the IEEE International Symposium on Intelligent Control*, pp. 340-347, 1989.

[2] S. Koenig and M. Likhachev, "Improved fast replanning for robot navigation in unknown terrain," *Proceedings of the IEEE International Conference on Robotics and Automation (ICRA)*, pp. 968-975, 2002.

[3] A. Kelly and B. Nagy, "Reactive Nonholonomic Trajectory Generation via Parametric Optimal Control", The International Journal of Robotics Research, Vol. 22, No. 7–8, pp. 583-601, July–August 2003.

[4] T. M. Howard, C. J. Green, and A. Kelly, "State Space Sampling of Feasible Motions for High-Performance Mobile Robot Navigation in Complex Environments", *Journal of Field Robotics,* 25(6–7), pp 325–345, 2008.

[5] T. K. Yeu, S. J. Park, S. Hong, H. W. Kim and J. S. Choi, "Path Tracking using Vector Pursuit Algorithm for Tracked Vehicles Driving on the Soft Cohesive Soil", *SICE-ICASE International Joint Conference Bexco, Busan, Korea,* Oct. 2006.

[6] T. Hellstrom, T. Johansson, and O. Ringdahl, "Development of an autonomous forest machine for path tracking", *Field and Service Robotics,* chapter 50, pp. 603–614, Springer, New York, 2006.

[7] J. Wit, C. D. Crane, and D. Armstrong, "Autonomous ground vehicle path tracking", *Journal of Robotic Systems*, vol. 21(8), pp. 439-449, Mar. 2004.

[8] G. Heredia and Anibal Ollero, "Stability of Autonomous Vehicle Path Tracking with Pure Delays in the Control Loop", *Advanced Robotics*, vol. 21, No. 1-2, pp. 23-50, 2007, Available: http://www.ingentaconnect.com/content/vsp/arb/2007/00000021/F00200 01/art00002.

[9] J. Morales, J. L.Martinez, M A. Martinez, and A. Mandow, "Pure-Pursuit Reactive Path Tracking for NonholonomicMobile Robots with a 2D Laser Scanner", *EURASIP Journal on Advances in Signal Processing,* vol. 2009, Article ID 935237, 10 pages.

[10] R. N. Jazar, *Vehicle Dynamics: Theory and Applications*, Springer, New York, 2008, p. 601.

[11] L. E. Ray, "Estimation of Terrain Forces and Parameters for Rigid-Wheeled Vehicles", *IEEE Transactions on Robotics*, vol. 25(3), Jun 2009.

[12] T. D. Gillespie, "*Fundamentals of Vehicle Dynamics*", Society of Automotive Engineers, Warrendale, 1992, pp. 347-355.